Lessons Learned from the Application of UAV-Enabled Structure-From-Motion Photogrammetry in Geotechnical Engineering

Dimitrios Zekkos, *Associate Professor, Department of Civil and Environmental Engineering, University of Michigan, Ann Arbor, Michigan, USA; email:* [*zekkos@geoengineer.org*](mailto:zekkos@geoengineer.org)

William Greenwood, *graduate student researcher, Department of Civil and Environmental Engineering, University of Michigan Ann Arbor, Michigan, USA; email:* [*wwgreen@umich.edu*](mailto:wwgreen@umich.edu)

Jerome Lynch, *Professor, Department of Civil and Environmental Engineering, University of Michigan, Ann Arbor, Michigan, USA; email:* [*jerlynch@umich.edu*](mailto:jerlynch@umich.edu)

John Manousakis, Surveying & Geomatics Engineer, ElxisGroup, Athens, Greece; *email:* [*jmanousakis@elxisgroup.com*](mailto:jmanousakis@elxisgroup.com)

Adda Athanasopoulos-Zekkos, *Associate Professor, Department of Civil and Environmental Engineering, University of Michigan, Ann Arbor, Michigan, USA; email:* [*addazekk@umich.edu*](mailto:addazekk@umich.edu)

Marin Clark, *Associate Professor, Department of Earth and Environmental Science, University of Michigan, Ann Arbor, Michigan, USA; email:* [*marinkc@umich.edu*](mailto:marinkc@umich.edu)

Kristen, L., Cook, *Postdoctoral Researcher, GFZ, Potzdam, Germany; email:* [*kristen.cook@gfz-potsdam.de*](mailto:kristen.cook@gfz-potsdam.de)

Charalampos Saroglou, *Senior Teaching & Research Associate, Department of Geotechnical Engineering, School of Civil Engineering, National Technical University of Athens, Athens, Greece; e-mail:* [*saroglou@central.ntua.gr*](mailto:saroglou@central.ntua.gr)

ABSTRACT: *The application of the Structure-from-Motion (SfM) methodology, as enabled by the growth of Unmanned Aerial Vehicle (UAV) technology, is expected to have significant impact in geotechnical engineering research and practice. SfM outputs are presented using selected geotechnical projects as examples, and include orthophotos, 3D point clouds, and three dimensional digital surface or terrain models. Repeated surveys allow for monitoring of deformation patterns at a cm-level resolution. The lessons learned from the application of the methodology at twenty-six sites that cover the breadth of geotechnical engineering practice, located in four countries (USA, Greece, Nepal, and New Zealand) and variable geologic environments are presented. It is shown that the methodology leads to an unprecedented level of mapping that covers large areas at high resolution. In addition to the high resolution models, SfM models are shown to be comparable in accuracy to other surveying techniques and mapping technologies such as light detection and ranging (LiDAR). The advantages and disadvantages of the methodology are also presented with the intent to facilitate the greater incorporation of this methodology in geotechnical engineering. The use of UAVs makes the methodology especially appealing for immediate post-disaster response as it enables the collection of optical data in areas that are inaccessible or unsafe.*

KEYWORDS: Structure-from-Motion, Unmanned Aerial Vehicles, 3D model, drones, disasters

SITE LOCATION: Geo-Database

INTRODUCTION

The methods used for surface characterization and monitoring of geotechnical systems are rapidly evolving. Conventional surveying methods have been expanded to include terrestrial and aerial laser scanning techniques as well as other remote sensing techniques, such as satellite-based optical imagery and interferometric synthetic aperture radar (InSAR) methods. Advanced remote sensing techniques significantly expand our capabilities to map, monitor and quantitatively assess the

performance of environmental and infrastructure geosystems (Rathje and Franke 2016). Site monitoring has also expanded from occasionally cumbersome, spatially-limited, and expensive wired sensors that require manual intervention for data acquisition and analysis, to remotely-operated possibly inexpensive wireless sensors. Wireless sensors can automatically collect and transfer data to processing centers for real-time monitoring where they are then used to guide operation decisions. A relatively new methodology in surface mapping and monitoring that is already attracting scientific attention and has numerous applications in geotechnical engineering is Structure-from-Motion (SfM) photogrammetry that is enabled by Unmanned Aerial Vehicles (UAVs). In this paper, the methodology is presented, followed by a database of a wide range of sites where the methodology was implemented by the authors. UAV-enabled SfM output results are presented using selected sites as example and lessons learned from the application of the methodology to these sites are presented to document the capabilities and limitations of the methodology when used in geotechnical engineering practice and research.

UAV-ENABLED STRUCTURE-FROM-MOTION PHOTOGRAMMETRY

Although arguably a number of technological, computational and scientific advances have contributed in the development of UAV-enabled Structure-from-Motion, two main advancements were key: A technological advancement, namely, the wide availability of small Unmanned Aerial Vehicles (sUAV) and a scientific advancement, Structure-from-Motion (SfM) photogrammetric computational methods. These are briefly reviewed herein.

The Technological Advancement: Unmanned Aerial Vehicles

UAVs, also known as Unmanned Aerial Systems or drones, have been used for many years for defense, surveillance and public safety purposes (Merino et al., 2006; Straub, 2014; Boucher, 2015). However, in the last decade, there has been an unprecedented growth in small UAVs (sUAVs), i.e., UAVs that weigh less than 25 kg (55 lbs). sUAVs are considered a rising new frontier in aviation (Wald, 2013) and have applications in many market sectors, disciplines and scientific fields, including construction, engineering, surveying, emergency response, product delivery, cinematography, and entertainment. The size of the combined market of sUAVs, estimated at several billions of dollars, has helped make the technology affordable for conventional applications in geotechnical engineering.

In the early stages of sUAV technology, flight control, flight time, and battery life were limited and affected the practical applicability of the technology in geotechnical engineering applications. Table 1 is a summary of the technological evolution of a popular quadrotor platform, the Phantom series. The Phantom 2 was released in December 2013, and its most recent iteration, Phantom 4 Pro, was released in December 2016. In these three years, as shown in Table 1, the UAV flight time increased, and reported flight range has practically quadrupled from less than 1 km to about 4 km and is now largely limited by government regulations and not technology. In addition, significant improvements were made to flight control, flight stability and collision avoidance of the aerial platform.

Table 1. Selected navigation, communication and data acquisition features of the Phantom Quadrotor platform series.

	Phantom 2	**Phantom 3 Pro**	**Phantom 4 Pro**
Released	December 2013	April 2015	November 2016
Flight Time	25 min	23 min	30 min
Maximum Speed	15 m/s	16 m/s	20 m/s
Camera Sensor	N/A*	1/2.3"	1"
Photo	N/A*	12 MP	20 MP
Video	N/A*	4k/30 fps**	4k/60 fps**
Flight Control Sensing	None	Downward position system (vision and sonar).	Stereo vision sensing. Side 3D infrared sensing.
Communication Range (FCC)	800 m	5000 m	7000 m
Navigation	GPS	GPS, GLONASS	GPS, GLONASS

*N/A: Not applicable.
**Fps: Frames per second

UAV technology has been continuously evolving. A recent review of UAV technology has been made by Lattanzi and Miller (2017), Colomina and Molina (2014) and Salami et al. (2014) and is beyond the scope of this paper. In general, there are two main types of battery-operated sUAVs: multi-rotors and fixed wing UAVs. Multi-rotors are typically smaller and able to take-off and land in constrained areas. They are very portable, and have the capability to remain stationary mid-air (i.e. hover) close to a target. Fixed wing UAVs have the ability to carry larger payloads, have typically greater battery life, greater flight range and travel at higher velocities. As a result, they can cover much larger areas, but must maintain greater distances from their targets and cannot hold position mid-air. The selection of one type (or model) of UAV is largely driven by the needs of the project with target area size, desired mapping resolution and portability being critical decisions, as discussed subsequently. Most UAVs are now equipped with a camera that has the capacity to collect still photos as well as video. The Phantom 4 Pro platform collects 20 MP photos and 4k (4096 × 2160 pixels) video, providing a resolution of approximately 1 cm/pixel from a height of 50 m. The ability to capture high-resolution imagery is a key requirement for reliable SfM application. Although current camera technology already offers data of unprecedented quality, the expected growth of camera technology will only improve the results and efficiency of SfM. For comparison, the ARGUS video surveillance platform that was developed in 2013 with funding from Defense Advanced Research Projects Agency (DARPA) and was mounted on a UAV, collects 1.8 GP images. That sensor can reportedly discern objects of about 15 cm (6'') on the ground at a height of 5,300 m (17,500 ft). Although the ARGUS platform is not available for conventional geotechnical practice, this technological innovation is indicative of the continued evolution of optical sensor technology that can be expected to eventually become part of civil engineering research and practice.

The Scientific Advancement: Structure-from-Motion Computation

Structure-from-Motion (SfM) photogrammetry is a computational imaging method that is based on the main principles of stereophotogrammetry (or stereoscopy). In stereophotogrammetry, the three dimensional positions of image features are derived by analyzing two or more photos collected from different positions that have significant overlap with each other. In traditional photogrammetric methods, the position and orientation of the camera sensor is known and is used to reconstruct the three dimensional geometry of the target. In SfM the target geometry and the sensor position and orientation are not known. Sensor position and orientation are solved simultaneously through an iterative, highly redundant bundle adjustment computational procedure using a set of features that are identified on multiple overlapping images. The SfM concept was first considered by Ullman (1979), but in its modern implementation, the SfM methodology was employed by Snavely et al. (2008) to reconstruct 3D targets using completely unordered imagery available on the internet. Since then, improvements in the accuracy and efficiency of SfM computations have been made (Schonberger and Frahm, 2016).

Structure-from-Motion Computation Methodology

The SfM methodology has been described in detail by a number of authors including Snavely et al. (2008), Westoby et al. (2012), and Cook (2017). Although SfM is a broad methodology for 3D reconstruction, when implemented with UAV-collected imagery, the methodology consists of the steps outlined in Fig. 1. This is the methodology followed in this study too. Field data collection involves the acquisition of overlapping imagery and the measurement of ground control points (discussed subsequently). The first step of the SfM computation methodology involves the identification of specific common features in overlapping imagery, a process known as feature extraction. Robust feature extraction from the imagery is required to produce acceptable results. Thus, image resolution, image overlap, and texture of the target will affect results. Theoretically, at least three images are necessary for each corresponding feature and thus an overlap in imagery of 70% or higher is recommended. Fig. 2 is a simplified example of this step where a UAV is shown collecting imagery of Diavas bridge that collapsed in Greece in 2016 (Zekkos et al. 2016). In each of three images, taken from different UAV positions, common features of the target are identified automatically or semi-automatically. In a more realistic implementation of the technique, many more features are automatically identified. Obtaining more than three images is also good practice and improves the results, but also increases computational cost. Different algorithms are used for feature extraction; most commonly the Scale Invariant Feature Transform (SIFT) as well as its derivatives (Shonberger and Frahm, 2016).

Incremental 3D Scene Reconstruction is then implemented for the input imagery to derive a "rough" three-dimensional geometry (i.e., a low density, or "sparse" point cloud) and estimates of the position and pose of the camera for each photo. This is executed through a sparse bundle adjustment process (Snavely et al., 2008) that includes algorithms for matching selected points, triangulation of 3D points, and the automatic elimination (or filtering) of moving objects that typically are identified by a large error in their position in different images compared to their neighboring points. To further improve the 3D model reconstruction accuracy, manual tie points, established as Ground Control Points (GCP) in the field, can be

identified throughout the photoset and be included for optimized solution processing of cameras' intrinsic (focal length, sensor size, principal point, lens distortion) and extrinsic (position, orientation) parameters.
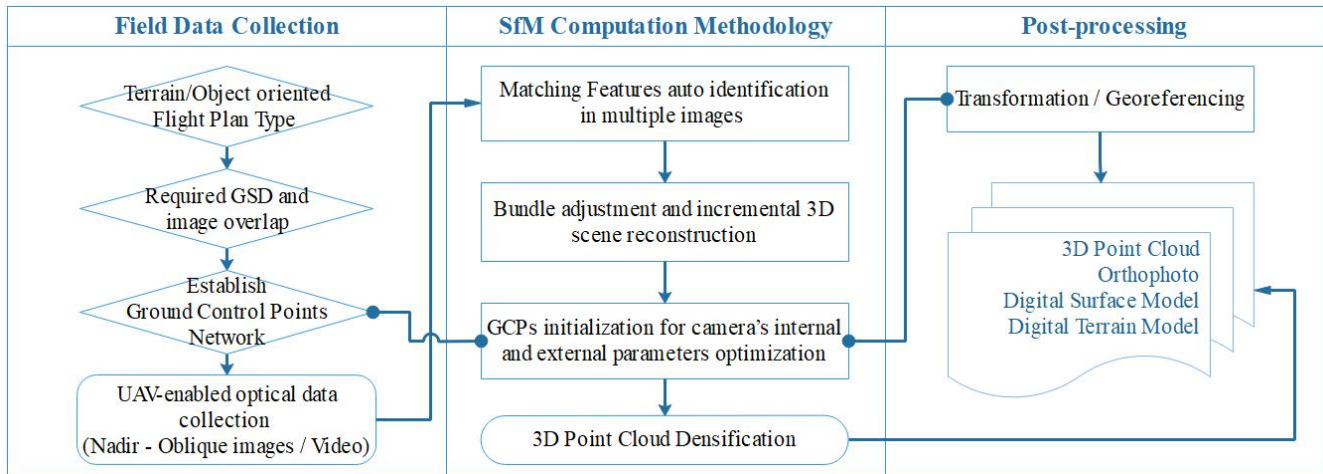

Field Data Collection	SfM Computation Methodology	Post-processing

Figure 1. Schematic of the UAV-enabled SfM process.

Subsequently, the derived sparse point cloud is significantly densified through stereoscopy algorithms that are used to create the final dense point cloud. The produced dense point cloud data has similarities to point clouds generated by other surveying technologies such as light detection and ranging (LiDAR) and terrain laser scanning (TLS).
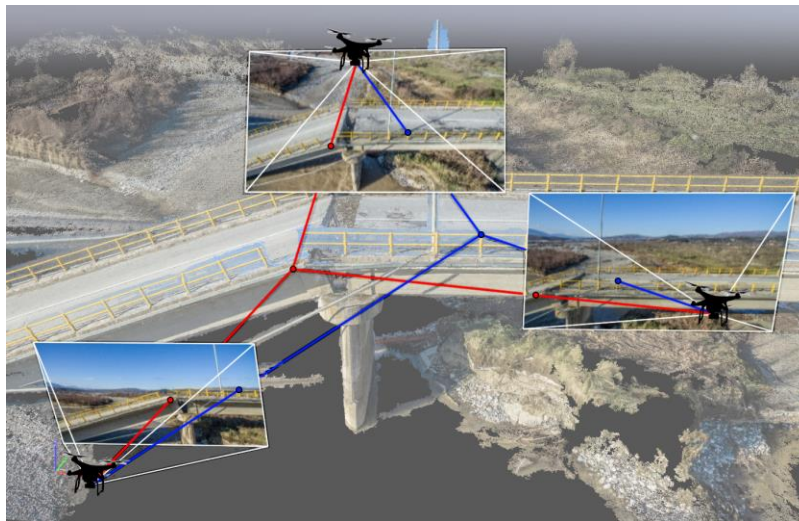

Figure 2. Illustration of the process of image collection and feature extraction
for the creation of a 3D model for Diavas bridge.

The last step involves the post-processing of the model and the creation of a digital surface model by identifying specific control points of "known" position in the 3D coordinate system (see also detailed description in "Ground Control Point Acquisition" section below). Theoretically a minimum of four such points are needed for positioning a model in a 3D coordinate system (three are required and a fourth as a check). Although prescriptive standards do not yet exist on the number of ground control points needed, four points are certainly not adequate for large areas and targets of complex geometry.

The density of the point cloud is a characteristic parameter of the resolution of the model and the number of points per volume is typically reported. A more common measure of the resolution of the model is the ground sampling distance (GSD), i.e., the distance between pixel centers on the ground surface. For example, a 10 cm GSD means that one pixel represents 10 cm on the ground. Thus, the higher the value of the GSD, the lower the resolution of the model. GSD is a key parameter because

features that are smaller or comparable size to the GSD cannot be discerned. At the same time, GSD is primarily affected by the flight parameters and the location of the camera compared to the surveyed target (extrinsic camera parameters), as well as the intrinsic camera parameters. This is illustrated in Fig. 3 where the achieved GSD as a function of distance from the target (flight height for horizontal targets) is shown for different types of cameras/UAVs. GSD is also affected, to a lesser degree, by other factors such as the computational routine details of the SfM methodology implemented and the texture and complexity of the target itself.
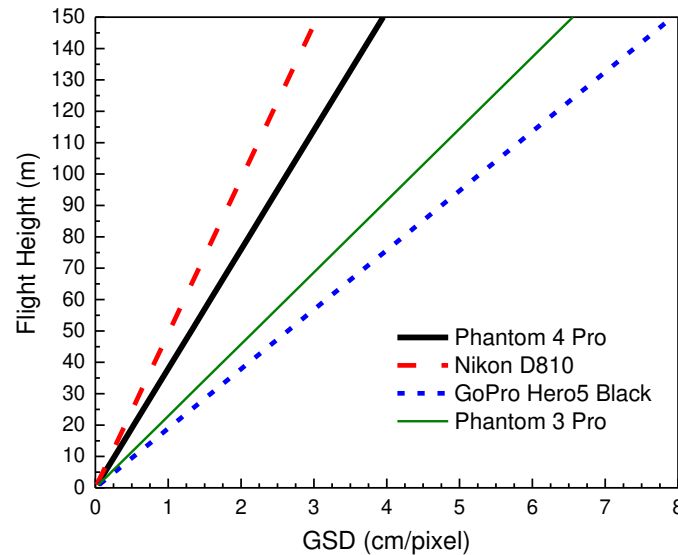

Figure 3. Range of GSD values vs flight height for different cameras used for UAV-based SfM

APPLICATIONS OF UAV-ENABLED PHOTOGRAMMETRY IN GEOTECHNICAL ENGINEERING

The earliest application of UAV-enabled photogrammetry in geotechnical engineering literature is less than four years old (Rollins et al. 2014), although the published record in geosciences extends to about six years (Niethammer et al. 2012; Viles, 2016) and in the broad civil engineering field (Rathinam et al., 2008) to less than a decade. UAV-enabled imagery has also been used for several years for qualitative assessments without the implementation of SfM photogrammetry (e.g., Murphy et al. 2015, Hashash et al. 2015, Siebert and Teizer, 2014). A list of geotechnical applications considered is provided in Table 2, and include infrastructure, such as dams and foundations (Zekkos et al. 2016), transportation infrastructure (Brooks et al. 2014) and deep excavation monitoring (Fleming et al. 2016).

Table 2. Types of geotechnical applications considered in the literature.

Type of Application	References
Rock Characterization	Stumpf et al. (2013); Bemis et al. (2014); Vasuki et al. (2014); Salvini et al. (2015); Greenwood et al. (2016); Vollgger and Cruden (2016)
Erosion	d'Oleire-Oltmanns et al. (2012); Neugirg et al. (2016); Hamshaw et al. (2017)
Landslides	Niethammer et al. (2012); Lucieer et al. (2014); Take (2015); Turner et al. (2015); El Mohtar et al. (2016); Greenwood et al. (2016); Zekkos et al. (2016); Zekkos et al. (2017)
Rockfall	Manousakis et al. (2016), Saroglou et al. (2017), Saroglou et al. (2018)
Foundations	Zekkos et al. (2016)
Dams	Zekkos et al. (2016)
Excavations	Hugenholtz et al. (2014); Siebert and Teizer (2014); Tong et al. (2015); Fleming et al. (2016)
Liquefaction	Rollins et al. (2014); Zekkos et al. (2016); Franke et al. (2016)
Ground Improvement	Franke et al. (2017)
Fault Rupture	Zekkos et al. (2018)

UAV-enabled photogrammetry has been implemented as part of geotechnical site reconnaissance in response to natural disasters and as a tool to replace traditional displacement measurements in the field (e.g., Greenwood et al., 2016; Zekkos et al., 2016; Kayen et al. 2016, Franke et al., 2017). Rollins et al. (2014) generated a 3D model of liquefaction damage of a port pier following the M8.2 Iquique, Chile, earthquake. A UAV-mounted camera was also used by the reconnaissance team to collect images and produce cm-scale 3D models of the Tana Bridge and liquefaction-induced displacements along the adjacent Tana River. Franke et al. (2016) compared UAV-based measurements of lateral spreading at the two liquefaction sites described in Rollins et al. (2014) against measurements using traditional field methods. Zekkos et al. (2016) deployed UAVs within 48 hours to map various failure sites following three natural disasters (an earthquake, a landslide and a flood) in Greece. Field deployment required only a few hours to map the target sites at cm-scale resolution. The ability of UAVs to cover large areas and reach sites with limited accessibility has made them also appealing for investigating landslides, especially following earthquakes. Following the 2015 Nepal earthquake, Greenwood et al. (2016) used UAVs to map landslides. Zekkos et al. (2017) mapped several km^2 of area that was heavily impacted by landsliding in the island of Lefkada, in Greece following the November 17th 2015 earthquake. Additional landslide investigations have been conducted by Niethammer et al. (2012), Turner et al. (2015), El Mohtar et al. (2016) as well as Lucieer et al. (2014) who with recurrent deployments developed cm-scale 3D point clouds and derived landslide deformations or displacements. Saroglou et al. (2017) and Manousakis et al. (2016) mapped two rockfall sites from the Cephalonia 2014 and Lefkada 2015 earthquake. The developed DSM was used to identify the rockfall trajectory, namely the rolling portion and rock bouncing locations during the event, and as input in rockfall analyses. Saroglou et al. (2018) used the rock fall mapping in Lefkada to back-calculate numerically the coefficients of restitution based on the rock bouncing locations.

UAV-collected imagery has been used for the three dimensional characterization of rock masses (e.g., Stumpf et al., 2013; Bemis et al., 2014; Salvini et al., 2015; Greenwood et al., 2016; Vollgger and Cruden, 2016), since UAV-enabled SfM is an obvious extension of terrestrial photogrammetric techniques that are well established for imaging rock masses in three dimensions in structural geology applications (Bemis et al., 2014). Emphasis has been placed on identifying and measuring discontinuities to quantify spatial variations and acquire geomechanical parameters. Vasuki et al. (2014) employed several image processing techniques to identify the orientation of rock mass discontinuities. Approaches with automated 2D and 3D image processing techniques are expected to grow as automation is a desirable aspect of large-scale monitoring and mapping with UAVs.

It is appropriate to make special reference to geomorphic mapping efforts, where UAV-mounted cameras are found to be particularly powerful for geomorphological mapping of large areas rapidly and acquiring data in difficult to reach locations (Serban et al., 2016, De Haas et al. 2014, James et al., 2017). For these type of applications, fixed-wing UAVs have been used (Hugenholtz et al. 2013, d'Oleire-Oltmanns et al. 2012). The approach of repeating UAV-based surveys to monitor displacement, or volume changes over time can also be applied to erosion (Hamshaw et al., 2017, Neugirg et al. 2016).

METHODOLOGY FOLLOWED IN THIS STUDY

Field Sites

A total of twenty-six (26) field sites where UAV-enabled SfM was implemented as part of this study, are summarized in Table 3. The sites summarized were selected from a broader list of sites documented by the authors to represent a diverse range of geographic conditions, objectives, and type of targets. The sites are located in the United States, Nepal, New Zealand and Greece. Deployment took place primarily in response to several natural disasters, including earthquakes, floods, and monsoons, but also as part of broader mapping efforts of the target sites. The list includes diverse targets that span the breadth of geotechnical engineering practice and include steep cliffs (site 1), soil slides, rock slides and debris flows (site 2, 4-8, 10, 11, 17, 26), rockfalls (site 9, 12), ports (site 13, 14), a levee (site 22), a failed structure (site 15), a fault rupture site (site 16), a bridge collapse (site 18), a dam failure (site 19), a retaining wall (site 21), a quarry (site 25) and different bare ground conditions, such as coastlines (site 3), sloping ground (site 9), sub-urban areas (site 23), as well as cultural heritage sites (site 20, 24). The deployment was generally successful in all these sites and conditions, highlighting the ability of the methodology to generate reliable outcomes for a wide range of geo-applications and conditions.

UAVs Deployed

Field expeditions were conducted with quadrotor UAVs of the Phantom series (Phantom 2 Vision+, Phantom 3 Pro and Phantom 4 Pro) as well as the octorotor 3D Robotics X8 platform that was equipped with a GoPro camera. Empirically, the flight team noticed significant improvement in UAV stability, control, and communication with the base station as the

technology advanced from the Phantom 2 to the Phantom 4 in these three years. These improvements had a direct positive effect on productivity and efficiency in the field and on data quality. With the exception of site 1, 2 and 3, the sites listed in Table 1 were mapped with Phantom 3 Pro.

Table 3. Selected sites mapped using UAV-enabled Structure-from-Motion. Coordinates of each site are available through the journal's geographic database.

Site ID	Site Description	Location	Total Flight Duration, min:sec	Approximate Camera Distance from Target, m	3D Area covered, m^2	Average GSD, cm/pixel	Passes
1	Cliff	Hawaii, USA	60:00	10	700	0.4	1
2	Cobbles	Hawaii, USA	8:00	6	345	0.2	1
3	Coastline	Hawaii, USA	9:00	13	1320	0.4	1
4	Rockslide 1	Nepal	5:00	40	3500	1.7	1
5	Rockslide 2	Nepal	10:00	28	10000	1.2	1
6	Complex or Rockslides	Nepal	9:00	200	329100	10.8	1
7	Terrace failure	Nepal	4:00	20	1400	0.9	1
8	Debris flow	Nepal	13:26	57	60700	2.5	1
9	Rockfall sloped area	Lefkada, Greece	38:50	114	1223160	5.0	1
10	Egkremnoi Landslide Area	Lefkada, Greece	41:10	143	637000	6.3	2
11	Platys Yalos Landslide 2	Lefkada, Greece	15:00	183	935835	6.9	1
12	Rockfall	Cephalonia, Greece	13:10	150	340900	7.1	1
13	Lixouri Port	Cephalonia, Greece	11:20	93	87300	3.9	1
14	Argostoli Port	Cephalonia, Greece	19:27	84	129000	3.9	1
15	Failed Campaneli	Cephalonia, Greece	11:40	10	154	0.5	2
16	Fault Rupture site	New Zealand	12:00	50	135600	2.3	1
17	Landslide site	New Zealand	28:00	94	654365	3.7	2
18	Scoured Bridge	Greece	30:00	18	5382	0.7	2
19	Irrigation Dam Collapse and flooded area mapping	Greece	70:00	62	390000	2.15	1
20	Anonymous Archaeological Site	Greece	125:00	61.1	759000	2.3	1
21	Retaining wall	Patras, Greece	9:20	40	30890	2.1	2
22	Levee	St. Louis, MO, USA	27:00	36	42000	1.6	1
23	Sub-urban area	Marousi, Greece	8:00	54	87344	1.7	1
24	Cliffed historical site	Chios, Greece	7:00	83.5	58000	2.15	1
25	Quarry	Penteli, Greece	10:00	55	72000	2.8	2
26	Moira landslide	Achaia Greece	40:00	120	790000	3.9	2

Computational Methodology

The computational methodology described previously and summarized in Figure 1 was followed to analyze the sites listed in Table 1. The methodology was implemented using a number of alternative SfM software, but primarily the commercial software programs Pix4D and Agisoft Photoscan were used. The various SfM software were found to generate comparable results.

RESULTS

In this section, the different types of outputs that can be generated by application of UAV-enabled SfM are presented with the intent to promote an improved understanding of what can be expected to be achieved in geotechnical engineering practice. The purpose of UAV deployment varied for the different target sites listed in Table 3 and selected examples of the generated results are presented subsequently. In the following, the emphasis is not on qualitative assessments, which can be made directly with the collection of the vision data, but on outcomes that are based on quantitative assessments.

High-Resolution Orthophotos

Orthophoto is an image, or an assembly of images, that has been geometrically corrected (a process known as orthorectification) so that the scale of the orthophoto is uniform and allows for direct measurements of dimensions on it. Orthophotos are most commonly presented in plan view, but this perspective is not a requirement. Fig. 4 is an orthophoto and a digital surface model (DSM) of the failure of Sparmos dam in Greece (site 19 in Table 3). The dam had clear signs of distress due to piping and underseepage. On March 26 2016, a 35 m in width dam section collapsed and the impounded water was released abruptly causing erosion downstream to depths greater than 2 m in places. The flooded area was estimated to be 100,000 m^2. Flight operations lasted 70 min at an average height above target of about 62 m and covered an area of 310,000 m^2. The ground sampling distance was 2.15 cm/pixel. More details on this site are provided in Zekkos et al. (2016). Fig. 4c compares a plan view of the downstream portion of the dam away from the main breach as collected by the UAV, to the Google Earth imagery from 29/8/2015, i.e., about seven months earlier (Fig. 4d). The difference in resolution is evident with the UAV imagery clearly illustrating soil flows, and disturbance that cannot be as clearly observed in the earlier Google Earth satellite imagery.
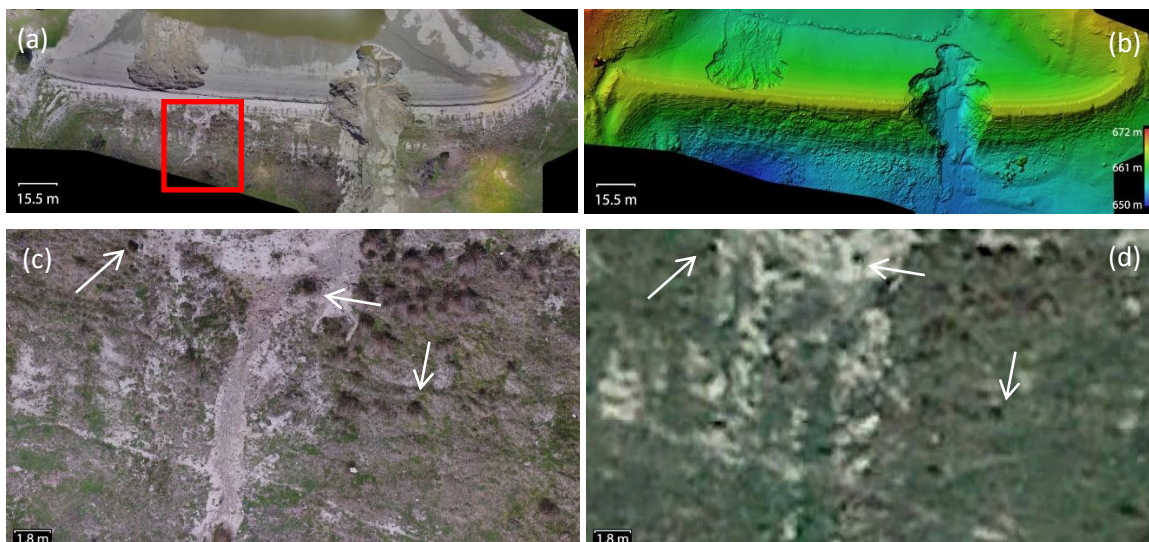

Figure 4. (a) Orthophoto of the 3/26/2018 underseepage and piping failure of Sparmos Dam, Greece and flooded area; (b) digital surface model (DSM) of the dam; (c) view of boxed area in (a) based on UAV-based orthophoto (plan view) illustrating surface disturbance in the downstream side of the dam; and (d) view of the same area as shown in Google earth image based on 2.5 m SPOT satellite imagery (dated: 29/8/2015). White arrows indicate identical features in the imagery for comparison.

3D Point Cloud Creation and Direct Displacement Measurements

The development of 3D point clouds is the raw output of the SfM methodology. Depending on the objective of the project, the results can be presented as 3D point clouds, or in some cases as an interpolated digital surface model (DSM) or digital terrain model (DTM) (2.5D raster maps with elevation information encoded in each pixel). An example of UAV data at a rural archaeological site (site 20) in the three formats is shown in Fig. 5 with color-coded altitude visualization. 2.5D raster surface models are developed by interpolation between 3D points and rasterization of altitude information along a XY Grid with specified pixel dimensions. They are particularly useful in creating surfaces that are easier to visualize and process (for example to generate cross-sections), and generally require less computational power to manipulate compared to TIN -vector interpolated- models. DSM represents a model of the surface including all ground, structures, trees and other features. DTM is a model where only the points that correspond to the terrain (ground) are taken into account. In cases of dense vegetation cover, developing a DTM from SfM may be practically impossible. However, in places where vegetation is not dense, a DTM can be developed using automatic, semi-automatic or manual techniques to remove vegetation (Gruszczynski et al., 2017; Pirotti et al., 2013; Meng et al., 2010).
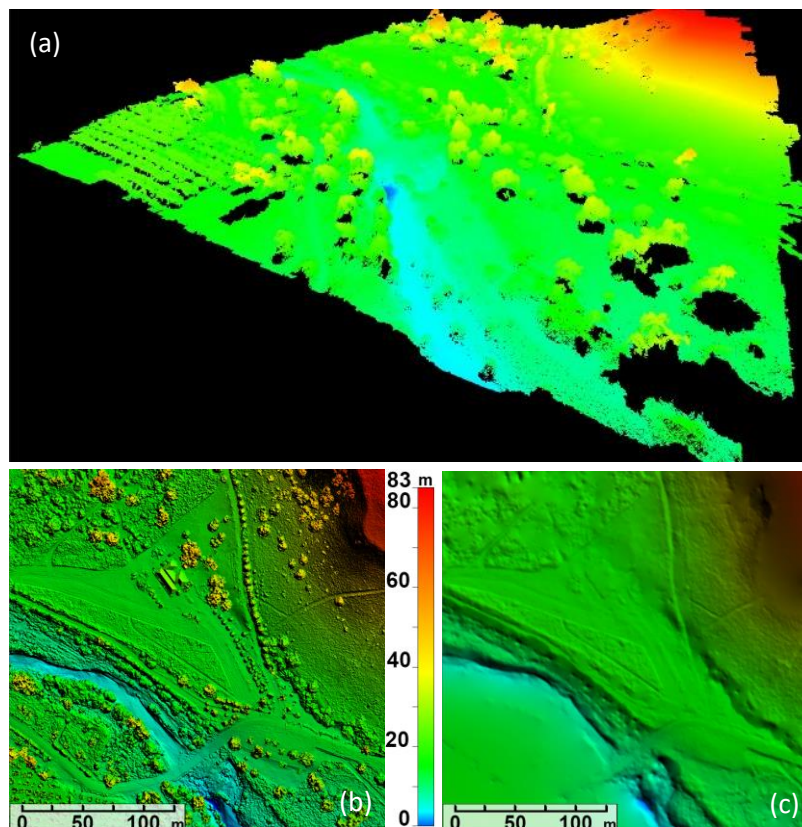

Figure 5. (a) 3D point cloud, (b) Digital Surface Model (DSM), (c) Digital Terrain Model (DTM) generated by a UAV at site 20.

Analysis of the 3D point clouds allows for direct displacement measurements. An example of this is shown for the case of the bridge of Diavas (site #18), described in more detail in Zekkos et al. (2016). Scour below the footing of a bridge pier resulted in the displacement and rotation of the pier and caused the collapse of the two simply supported bridge decks. Deployment of the UAV at that site lasted 30 minutes. Due to the complex, three dimensional geometry of the failure, 2 passes were executed with different camera orientations so that the top, sides and underside of the bridge can be accurately mapped. The processed data resulted in a 3D model of the entire bridge. Of particular interest was the displaced bridge pier. Since the decks are of predefined length, the initial location of the bridge pier was well established, and thus, direct measurements of the final location of the bridge pier generated by SfM allowed for an accurate assessment of the bridge pier movement, as shown in Fig. **6.** It was found that the base of the bridge pier displaced 1.38 m along the bridge axis, 0.91 m perpendicular to its axis, and was subjected to a horizontal rotation of 5.7°, and a vertical inclination of 29.1°. The vertical displacement was measured at 1.77 m compared to the original position of the pier. To execute these measurements, the team remained at a safe distance from the failure location and the river flow that was at a high elevation at the time of deployment.
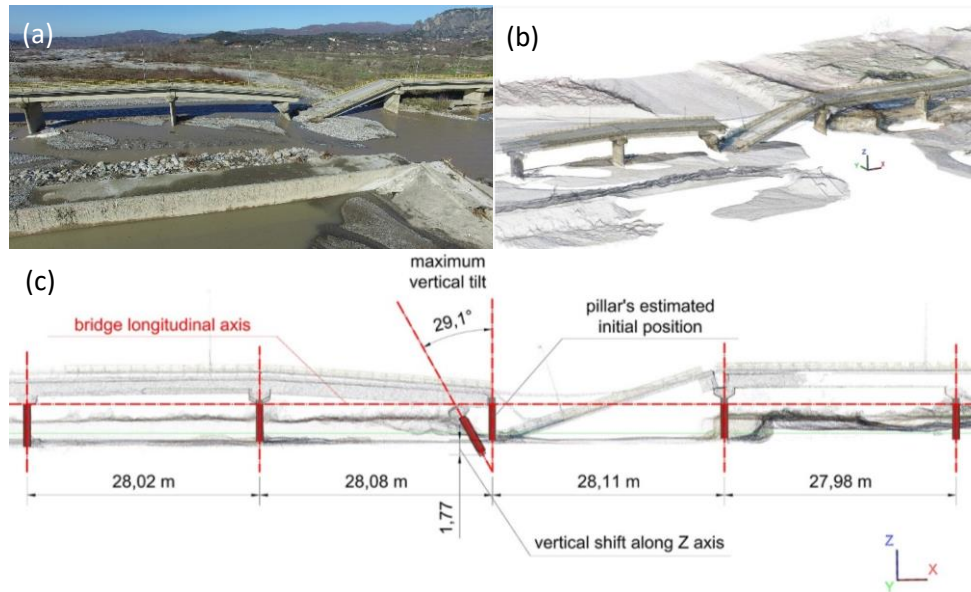
Figure 6. Diavas Bridge (site 18) collapse in Greece due to scour. (a) aerial photo; (b) 3D point cloud; (c) longitudinal cross-section through 3D point cloud with displacement measurements.

Generation of DSM for Surface Creation and Geometry-Based Analysis

The 3D point cloud can be used to directly measure distances or execute other assessments. A key characteristic of the SfM point clouds compared to standard LiDAR or TLS point clouds is that the points do not only have geometric attributes (i.e., x, y, z, coordinates), but also image attributes, i.e., Red-Green-Blue (RGB) components. While RGB values can be incorporated into LiDAR or TLS point clouds, this requires the use of an additional sensor. Interpolated digital surface models can also be used to facilitate assessments, such as the separation of a structure, tree, bush or other item, from the ground surface (terrain).

Once a DSM or DTM model has been developed, analysis can be executed. For example, if a pre-failure DSM is available, direct differencing between surfaces can be implemented to analyze the pre- and post-event geometry to estimate volumes as well as deformational patterns. Cross-sections through the surface model can also be developed to create a profile of the mapped geometry, and in the case of landslides, the profile geometry can be used as input in stability analyses. An example is shown in Fig. 7 for a landslide that was triggered in 2017 following a major precipitation event (site 26). Cross-section A-A' is cut through the center of the landslide and the change in topography is evident when the UAV model is compared to the pre-event 5 m DSM. No practical difference is observed for cross-section B-B' outside the landslide. It is important to note that the resolution in the differencing can only be as good as the resolution of the pre- and post-event DSM. In many cases, the pre-existing geometry is not available or is of inadequate resolution (i.e., too coarse). In cases of differencing, UAV surveys need robust measurements of ground control points (as discussed subsequently) to ensure that differencing does not lead to erroneous results.

Comparison of the before and after the landslide imagery is shown in Fig. 7d and 7e and is used to measure displacement direction and amount. Fig. 7d illustrates the satellite imagery before the landslide based on google Earth imagery, whereas Fig. 7e illustrates the after imagery where UAV imagery is overlain on the satellite imagery. Circles indicate common points in the two images. Red circles indicate initial points that moved due to landsliding and green circles, points that have not moved defining essentially the boundaries of the disturbed area. For the red points, in Fig. 7e, arrows indicate the final location of the point and the amount of horizontal displacement is shown. It is shown that the main mass of the landslide moved 60 m downhill (towards southeast). Portions on the side of the landslide have moved much less, in the order of 5-8 m and the amount of horizontal displacement reduces further back towards the crest of the landslide. This analysis provides a better assessment of the landslide kinematics, and if warranted, more points could be examined.

Differencing between the DTM from the national Cadastre prior to the landslide and the DSM developed from the UAV is shown in Fig. 7f. Some elevation differences are observed that are due to the accuracy and coarse resolution (5 m) of the Cadastre DTM and the presence of vegetation. However, the landslide is discernible as an increase in elevation ("mass gain" at the toe of the landslide, and a decrease in elevation ("mass loss") at the crest. Similar differencing analyses have been conducted by Zekkos et al. (2018) for landslide and fault rupture sites in New Zealand.
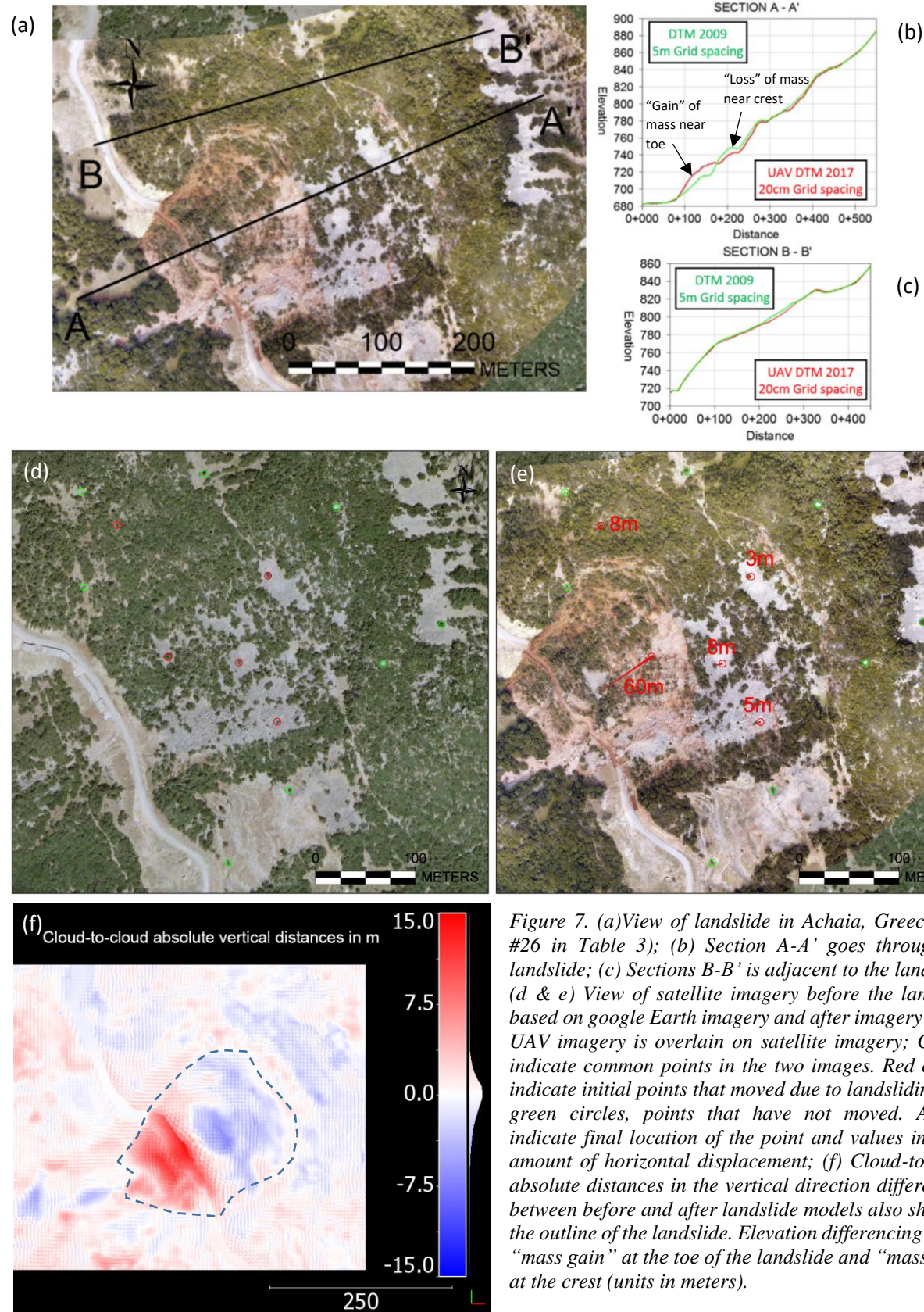
Figure 7. (a)View of landslide in Achaia, Greece (site #26 in Table 3); (b) Section A-A' goes through the landslide; (c) Sections B-B' is adjacent to the landslide; (d & e) View of satellite imagery before the landslide based on google Earth imagery and after imagery where UAV imagery is overlain on satellite imagery; Circles indicate common points in the two images. Red circles indicate initial points that moved due to landsliding and green circles, points that have not moved. Arrows indicate final location of the point and values indicate amount of horizontal displacement; (f) Cloud-to-cloud absolute distances in the vertical direction differencing between before and after landslide models also showing the outline of the landslide. Elevation differencing shows "mass gain" at the toe of the landslide and "mass loss" at the crest (units in meters).

Digital image analysis and feature recognition

The ability to generate three dimensional geometries that also have optical attributes, makes SfM outputs particularly amenable to further digital image analyses. Fig. 8 is an example of a 3D model of a block-paved surface that has cracked due to lateral movement of the seafront in the town of Vasiliki during the 2015 Lefkada earthquake. The highest resolution model has a GSD of 1.13 mm/pixel (Fig. 8a shows plan view and 8e shows oblique view). One can easily discern all the blocks as well as the joints between them. Models are also shown for less dense point clouds that result in lower resolution models with GSD that is two times (Fig. 8b and 8f) and four times (Fig. 8c and 8g) higher respectively. It is shown that as GSD increases the joints between blocks are becoming more difficult to discern. Fig. 8d is a photorealistic model of the cracked pavement. The arrow points to one of the bricks that was 115 mm in height. The measured height of the block from the model was 115 mm for the highest resolution model, 114 mm for the model with GSD of 2.27 mm/pi, and 103 mm for the model with GSD of 4.54 mm/pix, i.e., an error in height of about 10.4%. These obervations underline the importance of low GSD (high resolution) in reliably measuring dimensions of targets.
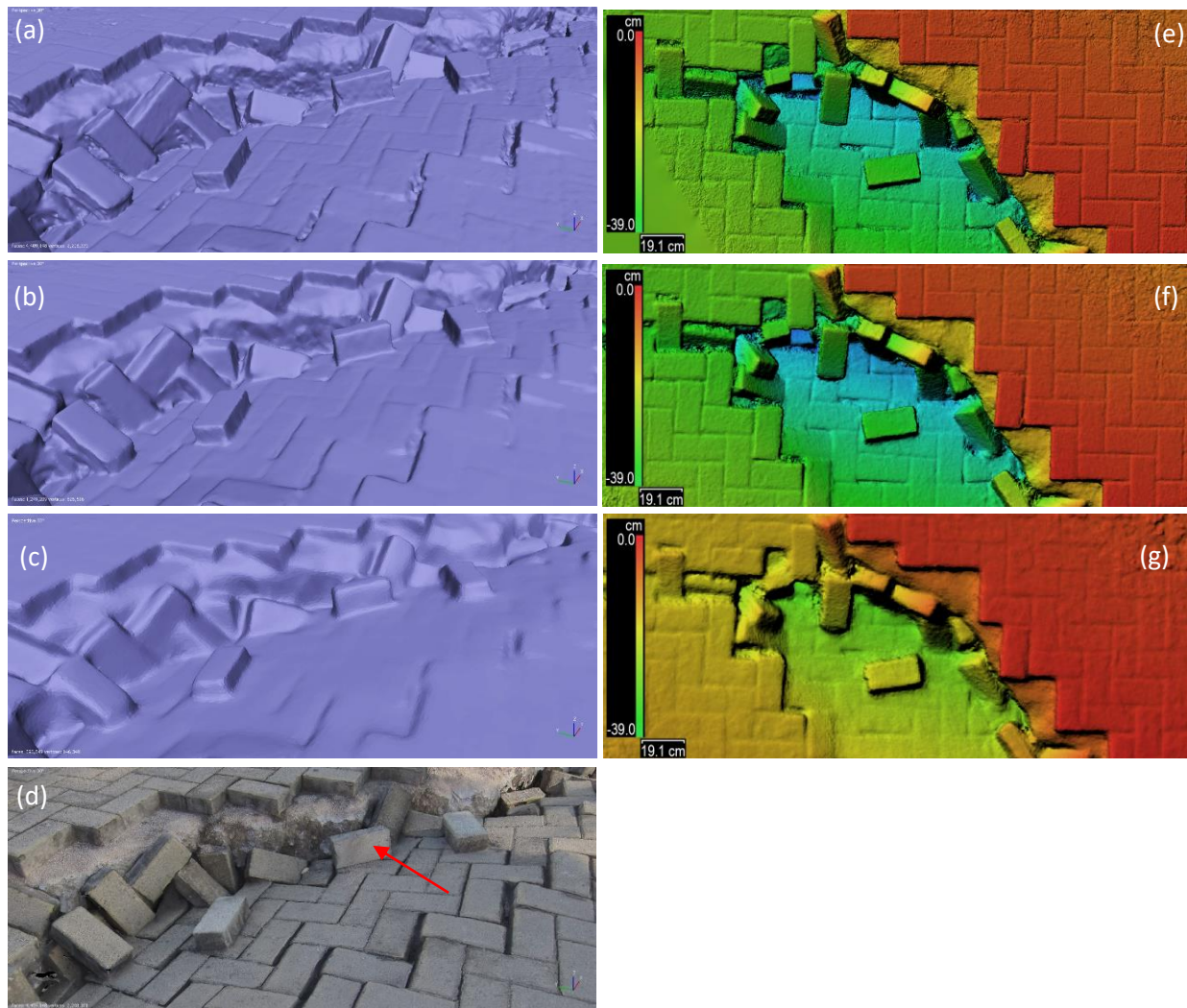

Figure 8. 3D model of cracked pavement with bricks at the Vasiliki port of Lefkada due to lateral movement of the seafront at a resolution of (a) 1.13 mm/pix (point density: 77.7 points/cm²); (b) 2.27 mm/pix (point density: 19.4 points/cm²); (c) 4.54 mm/pix (point density: 4.86 points/cm²). (d) photorealistic model of (a). Plan view at a resolution of (e) 1.13 mm/pix; (f) 2.27 mm/pix; (g) 4.54 mm/pix. Arrow points to brick being discussed in main text.

An additional example of digital imagery analyses that can be used to characterize the rock mass structure is shown in Fig. 9 for a landslide that was caused by the 2015 Nepal earthquake and was located about 28 km east of Kathmandu (site #5). The

crest of the landslide was located at a height of 150 m above its debris cone. The average slope of the landslide was 65°. The landslide was only accessible at the toe making any solely ground-based assessments limited. An overview of the rockslide is shown, as a point cloud, in Fig. 9a. Based on the UAV inspection, it was observed that the mechanism of the landslide was complex, consisting of shallow failure of a broken-up rock mass up-slope at the back and a structurally-controlled, planar failure at its base, which was tens of meters higher than the access road where the debris was deposited. Because of the access issues, a combination of GCP points (primarily on the landslide debris field and along the road) and laser points (distributed throughout the landslide mass) were used, as shown in Fig. 9b. Laser measurements targeted both the debris field and the landslide scarp and were used for either ground control points or ground check points. Note that ideally, one or two more ground control points should be collected at the top corners of the model. However, acquisition of such measurements from the toe in such a steep topography was impossible. The UAV was flown 40-80 m from the landslide scarp near the top of the slope. Subsequently, the UAV's camera was positioned 10-15 m away from the landslide to allow detailed assessments of the rock structure at critical locations. A layer of soil and extremely weathered rock was identified at the top 12 m of the slope. At lower elevations, the spacing and orientation of discontinuities can be discerned and was measured using the 3D point cloud. Based on the measurements of the bedding attitude using the 3D point cloud, the rock structure is dominated by foliation with an average strike of 255°, dipping at 20° to the northwest (Fig. 9c). This level of characterization of the landslide is made possible only through the use of a UAV and would not be reasonably feasible by other means (satellites, or ground-based assessments). Satellite imagery would not be of value in such steep topography and positioning a LIDAR unit on the ground with adequate view of the entire landslide would be challenging. Additional details about this landslide as well as another landslide (site #5 of Table 3) are provided in Greenwood et al. (2016).

Figure 9. (a) Overview of co-seismic landslide east of Kathmandu with distributed ground control points and laser points used as check points; (b) view of target on the ground at location shown by arrow in (a); (c) landslide back-scarp illustrating foliation of the rock; red lines indicate locations were foliation orientation was interpreted from the 3D model.

GROUND CONTROL POINT ACQUISITION

An important part of the development of reliable SfM 3D models is the pinning of the model at specific points of known location within a coordinate system. These are commonly referred to as ground control points (GCPs). Ground control points can be natural features, or other distinct engineered objects placed on the ground (such as the target shown in Fig. 9b) that can be easily identified in the collected imagery. Ideally, surveying of these targets using survey-grade equipment is conducted. Modern GPS systems can achieve a cm-level coordinate accuracy. In such cases, the created models can be comparable in accuracy with TLS data if sufficient number of GCPs are acquired. The GCPs then are positioned in space and the remaining model is appropriately scaled or stretched, to satisfy the positioning requirement of the GCPs.

It is always preferable to use numerous GCPs distributed throughout the surveying regions and especially near the areas of particular interest. If GCPs are not sufficiently spatially distributed, e.g., if they are only concentrated in one part of the modeled region, errors can accumulate as the distance from the nearest GCP increases and can become significant (Manousakis et al. 2016). Model errors also tend to increase as the geometry of survey targets become more complex, or the overlap among photos is reduced.

To assess model errors, check points are used. Check points are most commonly surveyed in a similar manner to GCPs, but are not used in the model development and georeferencing. Instead, comparison of the point cloud or DSM of the model

against check points provide a reliable error estimate of the model accuracy at the location of the check point. If several check points are also available, an estimate of average DSM accuracy can be derived. An example is shown in Fig. 10 for a DSM of a suburban area (site #23), where 7 ground control points are used, and 3 check points are used to assess the measurement error. The root mean square (RMSE) error is estimated to be 6.4 cm in the x-direction, 5.1 cm in the y-direction, and 2.9 cm in the vertical direction.

Positioning of the model in an absolute coordinate system is necessary especially if model comparisons are to be made at different times to monitor the evolution of a process. In other cases, positioning of the model in a relative coordinate system may be adequate. In those cases, measuring relative distances between targets, or placing scale bars on the ground so that they are visible in the imagery may be sufficient. As described earlier, in 3D model development of landslides in Nepal, model development and error assessment were conducted by placing targets on the ground surface at the accessible toe of the landslide, and by using a high-accuracy laser to measure distances from a tripod station to specific up-slope locations of the landslide that were not accessible.
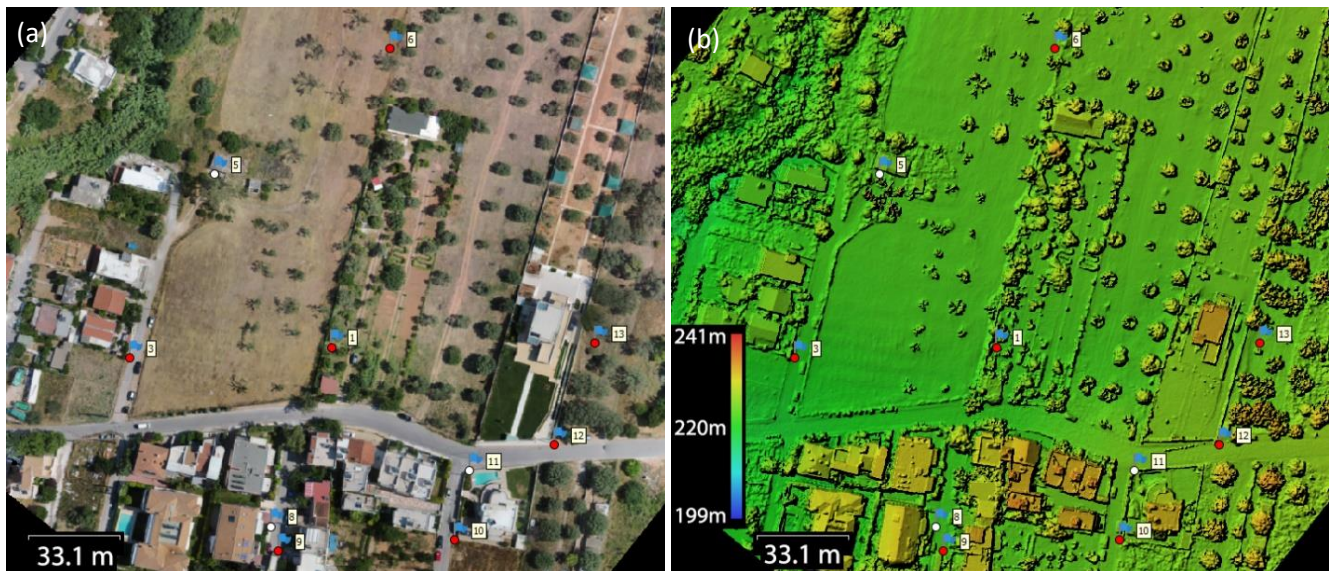

Figure 10. (a) Orthophoto and (b) DSM for sub-urban area (site #23) showing distributed ground control points and check points (with numbers).

3D MODEL ERROR ASSESSMENT

An important consideration when developing a SfM model is the potential errors associated with the creation of the 3D surfaces of the model, especially compared to other established techniques. Two comparisons of UAV-enabled SfM data against other established surveying methodologies are presented herein.

Fig. 11 compares the SfM model for a large sloped area (site #9), against the Hellenic national cadastre DTM. The digital elevation model of the national cadastre is based on photogrammetric methods using aerial photo strips and has a 5 m pixel size on the ground. The geometric accuracy of the product is RMSEz $\leq$ 2.00 m and absolute accuracy $\leq$ 3.92 m for a confidence level of 95%. The comparison with the UAV model is presented as a DEM of difference (DoD). Overall, a mean difference of 0.77 m and a standard deviation of 1.25 m is observed, which is well into the range of uncertainty of the national cadastre model itself.

Another example is shown for co-seismic landslides in Nepal along the Trishuli river (site #6). These were mapped simultaneously with a Riegl VZ-6000 LiDAR unit that has an accuracy of 15 mm and precision of 10 mm at 150 m range. The results are shown in Fig. 12 as a cloud-to-cloud comparison. As shown, the mean difference between the two clouds is 0.02 m with the standard deviation being 0.77 m, which is considered acceptable for a number of geotechnical purposes such as stability analyses and volume calculations. The largest differences are observed in areas of vegetation, the corners of the

model that are not considered reliable (because fewer images are being overlapped), as well as specific areas that were not as well visible by either the LiDAR or the UAV camera.

The findings from this study indicate that the SfM 3D models have comparable accuracy to other surveying techniques while they have also the advantages of high resolution and RGB attributes for the point clouds. These findings are consistent with previous studies that indicate that UAV-based photogrammetry can be a low cost alternative to LiDAR surveying for developing DSMs (Hugenholtz et al., 2013; Hugenholtz et al., 2014; Siebert and Teizer, 2014; Tong et al. 2015; Ruggles et al. 2016, Cook 2017, Zekkos et al. 2018).
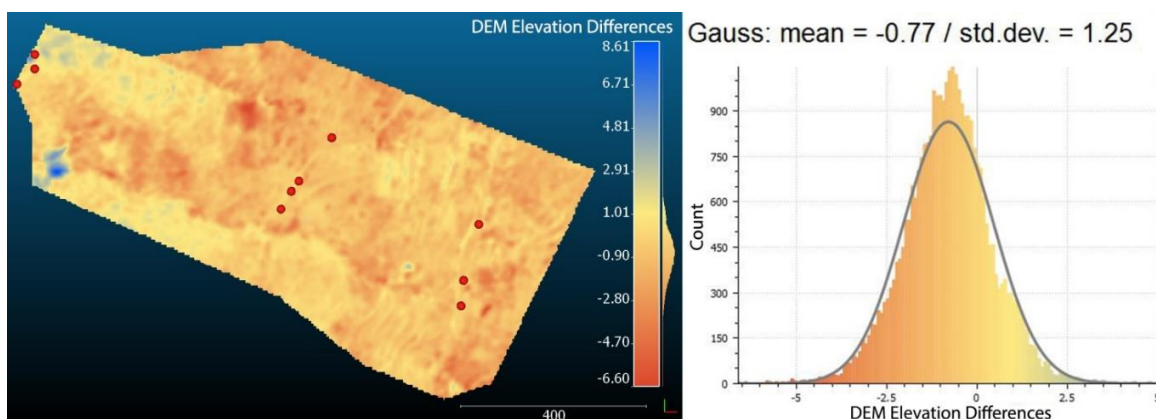

Figure 11. DEM of difference between UAV SfM DSM and Cadastre DTM for the Ponti sloping site (site 9).
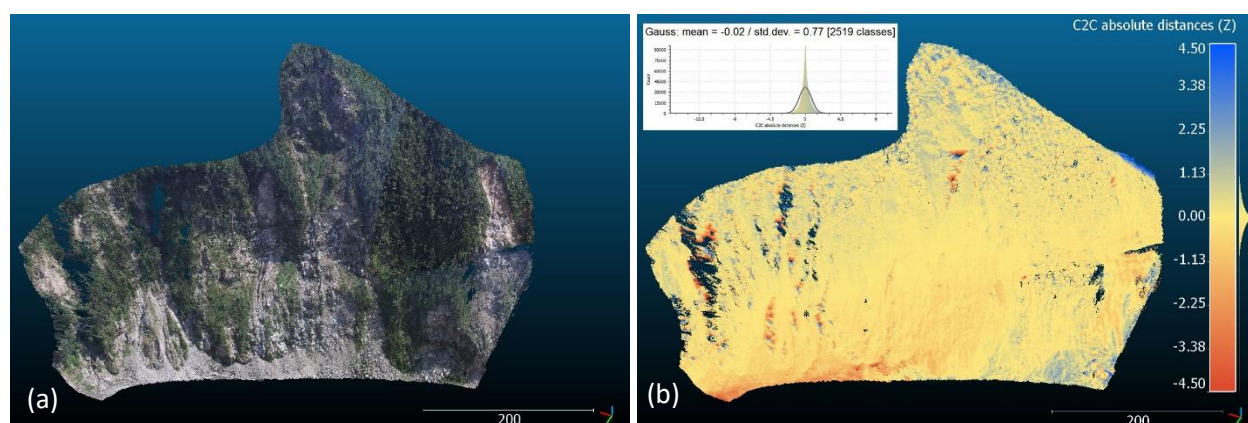

Figure 12. (a) View of SfM RGB 3d point cloud (scale in meters) and (b) cloud-to-cloud distance comparison (values in meters).

RECOMMENDATIONS FOR FIELD DATA ACQUISITION

Data acquisition in the field is critical and should balance the need to collect data against the risks associated with flying a UAV above the target. The following is a list of recommendations related to flying UAVs with the intent to develop SfM-based 3D models:

- The importance of flight parameters on the quality of optical data collected, cannot be overstated. The flight objective and route need to be clearly established before take-off. Once mid-air, the UAV should execute a specific plan that has accounted for weather conditions, and the time and energy needed for the UAV to return at its base safely. In selecting the flight objective, one should consider: (a) safety issues including battery life; (b) visibility of the target for a specific flight plan; (c) time of the day and weather conditions; (d) desired target resolution, all of which affect the flight parameters, especially distance to the target (for a given optical sensor) and (e) spatial distribution of GCPs and check points. An example of the influence of camera orientation is shown in Fig. 13 for site #23. The 3D point clouds of the targets for flights executed with camera pointing downwards only, are lacking data on the sides of the

buildings compared to the data generated with flights executed with camera pointing both downwards (in the first flight pass) and camera pointing obliquely and specifically 20 degrees upwards from vertical (in the second flight pass).

Figure 13. Comparison of point cloud data generated with (a) single pass and camera orientation pointing downwards only and (b) with double pass and camera orientation pointing downwards and obliquely. Notice the difference in the detail of the facades of the buildings, which is better captured by the oblique camera orientation.

- The flight path may be autonomous, or manual. Autonomous (or pre-programmed) paths allow the collection of imagery with preset overlap of photos, which is desirable to ensure the quality of data for the purposes of 3D model development. In addition, preset paths can streamline data processing. Manual flight operations, on the other hand, allow the pilot-in-command to control the flight in order to improve data quality, such as, change the camera orientation, move closer to the original or a new target of interest, and avoid obstacles.

- Weather conditions must be monitored for the safe execution of field deployment. Some UAVs are not equipped to properly operate in wet or even moist climate. Low temperatures can affect several sensors, including gyroscopes and accelerometers, and significantly reduce battery capacity. High winds, and especially gusty winds can affect flight stability and battery usage. In addition to the influence of weather conditions to safety considerations, deployment needs to take into account sunlight and its influence on the collected imagery. Depending on the time of the day, targets may become shaded, or reflective, affecting the quality of optical data generated. An overcast day with moderate light is preferable to bright, direct sunlight in many cases.

- An important consideration in field expeditions is the flight time required for the collection of adequate quality imagery data. Fig. 14 illustrates the relationship of flight time that was needed to collect the field data used for model development of the targets in Table 3. The flight time increases as the target area increases or the acquired model resolution increases (i.e., GSD decreases). It is found that the following relationship (R^2=0.71) is generally valid:

$$\frac{A}{GSD} = 2761.7 * t + 3215.3 \tag{1}$$

Where:

A is the 3D surface area being mapped in m^2
GSD is ground sampling distance as defined earlier in cm/pixel
t is the flight time in min.

This equation is valuable in providing an empirical estimate of the flight time necessary to collect data of specific resolution for a specific area. It is useful in coordinating flight plans for deploying a single or possibly swarms of UAVs over large areas. It should be noted that Site 1 is a site in Hawaii that used a Phantom 2 Vision+ platform that was less stable than the Phantom 3 when the winds were high and was also the very first site where the team deployed. Thus, this point is an outlier of the data shown, but also illustrates the effect of technology, pilot experience, and environmental conditions on the time required to survey a site.
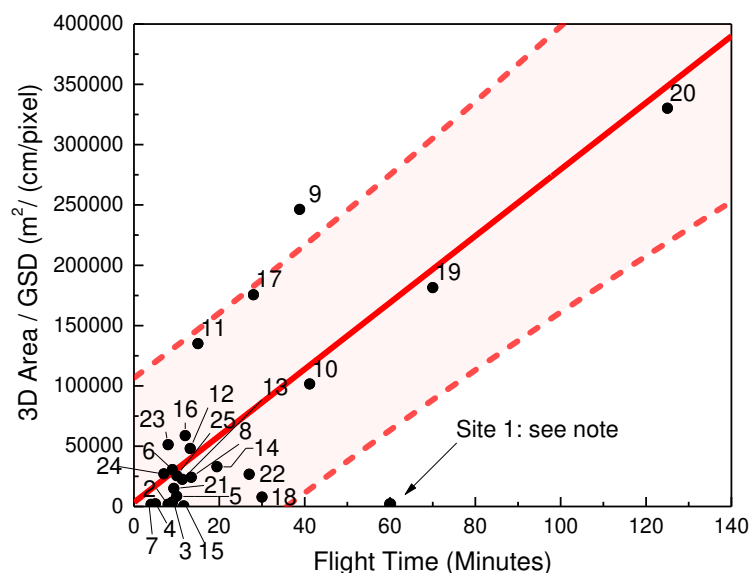
Figure 14. Relationship of the ratio of Area/GSD with flight time (dashed lines indicate 95% confidence interval ranges).

ADVANTAGES OF SFM MAPPING

The breadth of markets and sciences that UAVs already serve has permitted a reduction in the acquisition cost of UAV platforms that can be currently as low as $1000 for a platform with a 12 MP camera. Acquisition of a UAV with a high-resolution camera is significantly less expensive (in many cases by at least one order of magnitude) than the acquisition cost of a LiDAR or a TLS unit that generates similar (i.e., point cloud) data. In addition, deployment of UAVs is simpler and less expensive. It is also worth noting that the cost of acquiring a basic UAV-camera system is comparable, and in many cases lower, to hiring a helicopter to collect airborne photos for just one hour.

Among the many advantages of UAV-enabled SfM is the ability to access areas that are largely inaccessible. This advantage is particularly appealing in emergency response and geotechnical reconnaissance following natural disasters such as floods, earthquakes and hurricanes. Following natural disasters, collapsed structures, ground failure and other obstacles may affect accessibility. UAVs bypass obstacles and thus gain access to areas that would be unsafe or unreachable from the ground. Depending on the UAV platform used, access may be gained for a radius of several km. In these circumstances, portability is also key. Although some UAVs may be large, heavy, and more difficult to transport, many commercially available multi-rotor UAVs can weigh <2 kg and are small enough to be carried on a backpack (Zekkos et al. 2018). These platforms are ideal for data collection in remote areas.

The importance of the UAV ability to collect vision data from a range of perspectives (i.e., plan view, front oblique view, side view, etc.), as well as provide a closer view of a target feature, cannot be overstated. Many geological features are of large size and a view from the ground surface does not provide adequate understanding of the target site. Similarly, satellites provide primarily plan view perspective of the target, their resolution may not be adequate and their viewpoint may be obstructed by cloud coverage. An example demonstrating these advantages is the extensive landsliding that occurred during the November 17, 2015 earthquake in the island of Lefkada in Greece. Deployment took place only two days after the event and although large areas were completely inaccessible due to severe damage of the road network, UAVs were able to collect optical data of the landslides. Repeated deployment permitted mapping of the evolution of the landslides in that area (Zekkos et al. 2017).

LIMITATIONS OF SFM MAPPING

Flying one of the commercial UAV platforms is relatively easy to learn. However, experience is necessary to generate data of appropriate quality (spatial distribution and resolution) as data quality is affected by the sensor data (i.e., camera lens characteristics and camera positioning) as well as the flight characteristics (distance from the target, flight path, imagery overlap). Ground control points are critical to properly scale the point clouds and reduce distortions.

Depending on the size of the target and required resolution, processing time can be significant. Large area targets at high resolution are computationally intensive and may require many days of computations even with a powerful workstation. Error quantification is necessary to assess the reliability of results. As a rule of thumb, one field day with several flights requires about two to four days of office work. However, the level of effort at the office is also a function of the desired output and output derivatives.

Another key limitation that is inherent to the SfM process is the automatic identification of many distinct points in overlapping photos. Thus, in addition to the requirement for a minimum of 70% overlap in collected imagery, targets that lack texture may be very confusing to computational routines. In these cases, greater overlap (90%) may help model creation, although texture-lacking targets, such as asphalt pavements, water, and smooth uniform surfaces are difficult to nearly impossible to map reliably. Finally, an important disadvantage of SfM, when compared to other technologies that also generate point clouds, is the presence of vegetation. The methodology does not discern vegetation vs ground surface. Several computational routines exist for vegetation removal (Gruszczynski et al., 2017; Mongus and Zalik, 2012; Meng et al., 2010), and many of them involve smoothing, outlier removal, or selecting the lowest elevation point compared to its neighbor points in a point cloud. However, even such routines are not successful when the vegetation is thick, and completely obstructs view of the ground.

Finally, it is important to emphasize that regulations may impose significant restrictions to field operations. Regulations vary among countries and it is important to make sure that flight operations comply with local regulations and other flight restrictions. In the United States, Part 107 of the Federal Aviation Regulations require that flights are operated by a licensed UAV pilot, operations are restricted to line-of-sight and up to 121 m (400 ft) elevation. Flights above individuals and vehicles are also not allowed. These restrictions affect in some cases our ability to collected UAV-enabled SfM data, but also allow the successful execution of operations in other cases. In our experience, UAV regulations are continuously evolving in all countries as authorities are trying to accommodate this new aviation technology.

SUMMARY AND CONCLUSIONS

UAV-enabled Structure-from-Motion photogrammetry is shown to have numerous applications in geotechnical engineering. It can be used to generate high resolution (cm-level) orthophotos, as well as three dimensional point clouds and surface models that can then be processed to generate useful insights of geo-processes and the response of geotechnical infrastructure. Applications of the methodology are demonstrated for 26 different targets with an emphasis on diversity of projects and sites. The methodology is shown to be extremely powerful for a range of target sites, while at the same time, it is relatively inexpensive compared to alternative methodologies that generate similar type of data.

Despite its relatively short implementation record, the methodology is mature. It has the capacity to generate high resolution models with similar accuracy to conventional and advanced surveying technologies. Recommendations for field data acquisition are presented and an equation is provided to estimate flight time as a function of the model resolution (expressed using Ground Sampling Distance) and target size.

Application of the methodology in geotechnical engineering revolutionizes the quality, quantity and type of data that can be collected in the field and can be used for next generation modeling efforts that correctly account for the complex, three-dimensional and spatially distributed nature of geotechnical projects.

ACKNOWLEDGEMENTS

REFERENCES

Bemis, S. P., Micklethwaite, S., Turner, D., James, M. R., Akciz, S., Thiele, S. T., and Bangash, H. A. (2014). "Ground-Based and UAV-Based Photogrammetry: A Multi-scale, High-Resolution Mapping Tool for Structural Geology and Paleoseismology." *Journal of Structural Geology*, 69, 163-178.

Boucher, P. (2015). "Domesticating the Drone: The Demilitarisation of Unmanned Aircraft for Civil Markets." *Sci. Eng. Ethics*, 21, 1393-1412.

Brooks, C., Dobson, R. J., Banach, D. M., Dean, D., Oommen, T., Wolf, R. E., Havens, T. C., Ahlborn, T. M., and Hart, B. (2014). *Evaluating the Use of Unmanned Aerial Vehicles for Transportation Purposes*, Michigan Tech Research Institute Final Report, No RC-1616.

Colomina, I., and Molina, P. (2014). "Unmanned Aerial Systems for Photogrammetry and Remote Sensing: A Review." *ISPRS Journal of Photogrammetry and Remote Sensing*, 92, 79-97.

Cook, K. L. (2017). "An evaluation of the effectiveness of low-cost UAVs and structure from motion for geomorphic change detection." *Geomorphology*, 278, 195-208.

de Haas, T., Ventra, D., Carbonneau, P. E., and Kleinhans, M. G. (2014). „Debris-flow Dominance of Alluvial Fans Masked by Runoff Reworking and Weathering." *Geomorphology*, 217, 165-181.

d'Oleire-Oltmanns, S., Marzolff, I., Peter, K. D., and Ries, J. B. (2012). "Unmanned Aerial Vehicle (UAV) for Monitoring Soil Erosion in Morocco." *Remote Sensing*, 4, 3390-3416.

El Mohtar, C. S., Abou-Jaoude, G., Abdullah, C., and Harb, J. (2016). *The Kfarnabrakh Landslide of November 30th, 2015: A Geological and Geotechnical Evaluation of the Landslide and Risk of Future Failures*. GEER Association Report No. GEER-047.

Fleming, K. L., Hashash, Y. M. A., McLandrich, S., O'Riordan, N., and Riemer, M. (2016). "Novel Technologies for Deep-Excavation Digital Construction Records." *Practice Periodical on Structural Design and Construction*, 21(4).

Franke, K. W., Rollins, K. M., Ledezma, C., Hedengren, J. D., Wolfe, D., Ruggles, S., Bender, C., and Reimschiissel, B. (2016)." Reconnaissance of Two Liquefaction Sites Using Small Unmanned Aerial Vehicles and Structure from Motion Computer Vision Following the April 1, 2014 Chile Earthquake." *J. Geotech. Geoenviron. Eng.*, DOI: 10.1061/(ASCE)GT.1943-5606.0001647.

Franke, K. W., Nguyen, T., Shao, L., Bender, C., Wolfe, D., Hedengren, J. D., and Reimschiissel, B. (2017). "The Use of Unmanned Aerial Vehicles and Structure from Motion to Measure the Volume Change at a Deep Dynamic Compaction Site." *Geotechnical Frontiers 2017*, GSP 278, ASCE.

Greenwood, W., Zekkos, D., Clark, M. K., Lynch, J. P., Bateman, J., and Chamlagain, D. (2016). "UAV-Based 3-D Characterization of Rock Masses and Rock Slides in Nepal." *Proc. 50th US Rock Mechanics/Geomechanics Symposium*, Houston, TX.

Gruszczynski, W., Matwij, W., and Cwiakala, P. (2017). "Comparison of Low-Altitude UAV Photogrammetry with Terrestrial Laser Scanning as Data-Source Methods for Terrain Covered in Low Vegetation." *ISPRS Journal of Photogrammetry and Remote Sensing*, 126, 168-179.

Hamshaw, S. D., Bryce, T., O'Neil Dunne, J., Rizzo, D., Frolik, J., Engel, T., and Dewoolkar, M. M. (2017). "Quantifying Streambank Erosion Using Unmanned Aerial Systems at Site-Specific and River Network Scales." *Geotechnical Frontiers 2017*, GSP 278, ASCE.

Hashash, Y. M. A., Tiwari, B., Moss, R. E. S., Asimaki, D., Clahan, K. B., Kieffer, D. S., Dreger, D. S., Macdonald, A., Madugo, C. M., Mason, H. B., Pehlivan, M., Rayamajhi, D., Acharya, I., and Adhikari, B. (2015). *Geotechnical Field Reconnaissance: Gorkha (Nepal) Earthquake of April 25 2015 and Related Shaking Sequence*. GEER Association Report No. GEER-040.

Hugenholtz, C. H., Whitehead, K., Brown, O. W., Barchyn, T. E., Moorman, B. J., LeClair, A., Riddell, K., and Hamilton, T. (2013). "Geomorphological Mapping with a Small Unmanned Aircraft System (sUAS): Feature Detection and Accuracy Assessment of a Photogrammetrically-driven Digital Terrain Model." *Geomorphology*, 194, 16-24.

Hugenholtz, C. H., Walker, J., Brown, O., and Myshak, S. (2014). "Earthwork Volumetrics with an Unmanned Aerial Vehicle and Softcopy Photogrammetry." *Journal of Surveying Engineering*, 141(1).

James, M. R., Robson, S., d'Oleire-Oltmanns, S., and Niethammer, U. (2017). "Optimising UAV Topographic Surveys Processed with Structure-from-Motion: Ground Control Quality, Quantity and Bundle Adjustment." *Geomorphology*, 280, 51-66.

Kayen, R., Dashti, S., Kokusho, T., Hazarika, H., Franke, K., Oettle, N., Wham, B., Ramirez, J., Briggs, D., Guillies, S., Cheng, K., Tanoue, Y., Takematsu, K., Matsumoto, D., Morinaga, T., Furuichi, H., Kitano, Y., Tajiri, M., Chaudhary, B., Nishimura, K., Chu, C. (2016). *Geotechnical Aspects of the 2016 Mw 6.2, Mw 6.0, and Mw 7.0 Kumamoto Earthquakes*. GEER Report, 048, 163

Lattanzi, D., and Miller, G. (2017). "Review of Robotic Infrastructure Inspection Systems." *Journal of Infrastructure Systems*.

Lucieer, A., de Jong, A. M., and Turner, D. (2014). "Mapping Landslide Displacements using Structure from Motion (SfM) and Image Correlation of Multi-temporal UAV Photography." *Progress in Physical Geography*, 38(1), 97-116.

Manousakis, J., Zekkos, D., Saroglou, F., and Clark, M. (2016). "Comparison of UAV-enabled photogrammetry-based 3D point clouds and interpolated DSMs of sloping terrain for rockfall hazard analysis", *Int. Arch. Photogramm. Remote Sens. Spatial Inf. Sci.*, XLII-2/W2, 71-77.

Meng, X., Currit, N., and Zhao, K. (2010). "Ground Filtering Algorithms for Airborne LiDAR Data: A Review of Critical Issues." *Remote Sensing*, 2, 833-860.

Merino, L., Caballero, F., Martinez-de-Dios, J. R., Ferruz, J., and Ollero, A. (2006). "A Cooperative Perception System, for Multiple UAVs: Application to Automatic Detection of Forest Fires." *Journal of Field Robotics*, 23(3/4), 165-184.

Mongus, D., and Zalik, B. (2012). "Parameter-Free Ground Filtering of LiDAR Data for Automatic DTM Generation." *ISPRS Journal of Photogrammetry and Remote Sensing*, 67, 1-12.

Murphy, R. R., Duncan, B. A., Collins, T., Kendrick, J., Lohman, P., Palmer, T., and Sanborn, F. (2015). "Use of a Small Unmanned Aerial System for the SR-530 Mudslide Incident near Oso, Washington." *Journal of Field Robotics*, DOI: 10.1002/rob.21586.

Neugirg, F., Stark, M., Kaiser, A., Vlacilova, M., Seta, M. D., Vergari, F., Schmidt, J., Becht, M., and Haas, F. (2016). „Erosion Processes in Calanchi in the Upper Orcia Valley, Southern Tuscany, Italy based on Multitemporal High-Resolution Terrestrial Lidar and UAV Surveys." *Geomorphology*, 269, 8-22.

Niethammer, U., James, M. R., Rothmund, S., Travelletti, J., and Joswig, M. (2012). "UAV-based remote sensing of the Super-Sauze landslide: Evaluation and results." *Engineering Geology*, 128, 2-11.

Pirotti, F., Guarnieri, A., and Vettore, A. (2013). "Ground Filtering and Vegetation Mapping using Multi-Return Terrestrial Laser Scanning." *ISPRS Journal of Photogrammetry and Remote Sensing*, 76, 56-63.

Rathinam, S., Kim, Z. W., and Sengupta, R. (2008). "Vision-Based Monitoring of Locally Linear Structures Using an Unmanned Aerial Vehicle." *Journal of Infrastructure Systems*, 14(1), 52-63.

Rathje, E., M., Franke, K. (2017). "Remote sensing for geotechnical earthquake reconnaissance." *Soil Dynamics and Earthquake Engineering*, 91, 304-316.

Rollins, K., Ledezma, C., and Montalva, G. (2014). *Geotechnical Aspects of April 1, 2014, M8.2 Iquique, Chile Earthquake*. GEER Association Report No. GEER-038.

Ruggles, S., Clark, J., Franke, K.W., Wolfe, D., Hedengren, J.D., Martin, R.A., and Reimschissel, B. (2016). "Comparison of SfM Computer Vision Point Clouds of a Landslide from Multiple Small UAV Platforms and Sensors to a TLS based Model." *Journal for Unmanned Vehicle Systems*, DOI 10.1139/juvs-2015-0043.

Salamí, E., Barrado, C., and Pastor, E. (2014). "UAV Flight Experiments Applied to the Remote Sensing of Vegetated Areas." *Remote Sensing*, 6, 11051-11081.

Salvini, R., Vanneschi, C., Riccucci, S., Francioni, M., and Gullì, D. (2015). "Application of an Integrated Geotechnical and Topographic Monitoring System in the Lorano Marble Quarry (Apuan Alps, Italy)." *Geomorphology*, 241, 209-223.

Saroglou, C., Asteriou, P., Tsiambaos, G., Zekkos, D., Clark, M., Manousakis, J. (2017). "Investigation of two co-seismic rockfalls during the 2015 Lefkada and 2014 Cephalonia Earthquakes in Greece." *Proc. 3rd North American Symposium on Landslides*, Roanoke, Virginia, USA, 521-528.

Saroglou, C., Asteriou, P., Zekkos, D., Tsiambaos, G., Clark, M., and Manousakis, J. (2018). "UAV-based mapping, back analysis and trajectory modeling of a coseismic rockfall in Lefkada island, Greece." *Nat. Hazards Earth Syst. Sci,* 18, 321-333.

Schonberger, J. L., and Frahm, J. M. (2016). "Structure-from-motion revisited." *Proc. IEEE Conference on Computer Vision and Pattern Recognition*, 4104-4113.

Serban, G., Rus, I., Vele, D., Bretcan, P., Alexe, M., and Petrea, D. (2016). "Flood-Prone Area Delimitation using UAV Technology, in the Areas Hard-to-Reach for Classic Aircrafts: Case Study in the North-East of Apuseni Mountains, Transylvania." *Natural Hazards*, 82, 1817-1832.

Siebert, S., and Teizer, J. (2014). "Mobile 3D Mapping for Surveying Earthwork Projects Using an Unmanned Aerial Vehicle (UAV) System." *Automation in Construction*, 41, 1-14.

Stumpf, A., Malet, J.-P., Kerle, N., Niethammer, U., and Rothmund, S. (2013). "Image-based Mapping of Surface Fissures for the Investigation of Landslide Dynamics." Geomorphology, 186, 12-27.

Snavely, N., Seitz, S. M., and Szeliski, R. (2008). "Modeling the world from internet photo collections." *International Journal of Computer Vision*, 80(2), 189-210.

Straub, J. (2014). "Unmanned Aerial Systems: Consideration of the Use of Force for Law Enforcement Applications." *Technology in Society*, 39, 100-109.

Take, A. (2015). "Thirty-Sixth Canadian Geotechnical Colloquium: Advances in visualization of geotechnical processes through digital image correlation." *J. Can. Geotech.*, 52, 1199–1220

Tong, X., Liu, X., Chen, P., Liu, S., Luan, K., Li, L., Liu, S., Liu, X., Xie, H., Jin, Y., and Hong, Z. (2015). "Integration of UAV-Based Photogrammetry and Terrestrial laser Scanning for the Three-Dimensional Mapping and Monitoring of Open-Pit Mine Areas." *Remote Sensing*, 7, 6635-6662.

Turner, D., Lucieer, A., and de Jong, S. M. (2015). "Time Series Analysis of Landslide Dynamics Using an Unmanned Aerial Vehicle (UAV)." *Remote Sensing*, 7, 1736-1757.

Ullman, S. (1979). *The interpretation of visual motion*. Massachusetts Institute of Technology Press.

Vasuki, Y., Holden, E. -J., Kovesi, P., and Micklethwaite, S. (2014). "Semi-Automatic Mapping of Geological Structures using UAV-based Photogrammetric Data: An Image Analysis Approach." *Computers & Geosciences*, 69, 22-32.

Viles, H. (2016). "Technology and Geomorphology: Are Improvements in Data Collection Techniques Transforming Geomorphic Science?" *Geomorphology*, 270, 121-133.

Vollgger, S. A., and Cruden, A. R. (2016). "Mapping Folds and Fractures in Basement and Cover Rocks using UAV Photogrammetry, Cape Liptrap and Cape Paterson, Victoria, Australia." *Journal of Structural Geology*, 85, 168-187.

Wald, M. L. (2013). "Just Don't Call It a Drone." *New York Times*.

Westoby, M. J., Brasington, J., Glasser, N. F., Hambrey, M. J., and Reynolds, J. M. (2012). "'Structure-from-Motion' photogrammetry: A low-cost, effective tool for geoscience applications." *Geomorphology*, 179, 300-314.

Zekkos, D., Manousakis, J., Greenwood, W., and Lynch, J. (2016). "Immediate UAV-enabled Infrastructure Reconnaissance following Recent Natural Disasters: Case Histories from Greece." *Proc. 1st International Conference on Natural Hazards & Infrastructure*, Chania, Greece.

Zekkos, D., Clark, M., Cowell, K., Medwedeff, W., Manousakis, J, Saroglou, H., Tsiambaos, G. (2017). "Satellite and UAV-enabled mapping of landslides caused by the November 17th 2015 M$_w$ 6.5 Lefkada earthquake." Proc. 19th International Conference on Soil Mechanics and Geotechnical Engineering, Seoul, South Korea.

Zekkos, D., Manousakis, J., Athanasopoulos-Zekkos, A., Clark, M., Knoper, L., Massey, C., Archibald, G., Greenwood, W., Hemphill-Haley, M., Rathje, E., Litchfield, N., Medwedeff, W., Van Dissen, R.J., Kearse, J., Ries, W., Villamor, P., and Langridge, R.M., (2018). "Structure-from-Motion based 3D mapping of landslides & fault rupture sites during 2016 Kaikoura earthquake reconnaissance.", *Proc. 11th U.S. National Conference on Earthquake Engineering, Integrating Science, Engineering & Policy*, Los Angeles, California.

INTERNATIONAL JOURNAL OF GEOENGINEERING CASE HISTORIES

*The Journal's Open Access Mission is
generously supported by the following Organizations:*

Access the content of the ĪSSMGE Īnternational Journal of Geoengineering Case Histories at:
https://www.geocasehistoriesjournal.org